Journal of Materials Chemistry C

ROYAL SOCIETY OF CHEMISTRY

PAPER

View Article Online
View Journal | View Issue

Cite this: J. Mater. Chem. C, 2021, 9, 9584

Defect passivation and humidity protection for perovskite solar cells enabled by 1-dodecanethiol†

Dingchao He,[ab] Xiaoxiao Xu,[ab] Zheng Liang,[ab] Yuanjuan Niu,[ab] Yuan Sun,[a] Tulloch Gavin,[cd] Polycarpos Falaras *[c] and Linhua Hu *[a]

Received 14th April 2021,
Accepted 11th June 2021

DOI: 10.1039/d1tc01720a

rsc.li/materials-c

Multiple defects are likely to be produced during perovskite film preparation and exposure to a high humidity environment, which would negatively affect charge transport mechanisms and finally degrade the performance of perovskite solar cells (PSCs). In this work, we introduced a surface hydrophobic modifier, 1-dodecanethiol (DDT), to repair defects and enhance the moisture resistance of perovskite films. Through a series of tests, we found that defect repair by the thiol group in DDT can reduce trap density, inhibit non-radiative recombination and improve charge carrier transportation and extraction performance. In addition, benefiting from the excellent hydrophobicity of the dodecyl alkyl chain in DDT, both device efficiency and stability are significantly improved. Consequently, the device post-treated with DDT delivered a champion power conversion efficiency (PCE) of 20.89%, accompanied by outstanding long-range stability that exceeded 90% of its initial PCE after 1000 hours at a relatively high humidity of 80 ± 5% and without any encapsulation.

Introduction

As the most interesting technology of this era, organic–inorganic hybrid perovskite solar cells (PSCs), considered as the most promising next-generation photovoltaic devices, have attracted tremendous interest from researchers in the past decade due to their inherent outstanding properties, *i.e.*, long charge diffusion lengths and high light-harvesting coefficients.[1–3] Thanks to the efforts of researchers, the power conversion efficiency (PCE) of PSCs has been boosted to 25.5%.[4] The best performing PSC devices are usually based on mixed cation hybrid perovskite halide thin film materials, with the general formula of ABX_3 (A = methylammonium (MA), formamidinum (FA) or cesium (Cs) cations, B = Pb^{2+} and Sn^{2+}, and X = I^-, Br^- or Cl^-). Basically, a facile low temperature solution-based process can be used for the fabrication of perovskite films.[5,6]

However, FA_xMA_{1-x} PbX_3 mixed cation perovskite films suffer from intrinsic instability due to restricted thermodynamic equilibrium, causing significant X-type atom (I, Br) vacancy (halide vacancies) defects at the surface and at the inevitably grain boundary (GB) defects.[7–9] In polycrystalline perovskites, halide vacancies further provoke the destruction of the PbX_6 octahedral arrangement and create uncoordinated Pb^{2+} defects.[10] In addition, FA_xMA_{1-x} PbX_3 mix-cation perovskite films are unstable under humid conditions, which subsequently results in the degradation of the holistic device.[11] In fact, deterioration of FA_xMA_{1-x} PbX_3 films with substantial defects was observed upon exposure to ambient atmosphere, subsequently leading to poor cell stability and efficiency decline.

In previous studies, tremendous efforts including additive (dopant) strategies or post-treatment engineering have been exploited to obtain devices with superior performance, such as Cl^- ions,[12] Cu(thiourea)I[13] or thiol ligand.[14] Significant efficiency enhancement and stability improvement were achieved by using interface engineering methodologies,[15] including molecular dyes,[16–18] porphyrins,[19] graphene oxide[20] and transition metals.[21] Other approaches use ammonium cations[22,23] as passivators to improve the moisture tolerance of PSCs. By introducing one-dimensional (1D)[24] and two-dimensional (2D) stacking layers onto three-dimensional (3D) perovskites, the stability of PSCs was effectively improved.[25] The above works have effectively modified the perovskite film, but the waterproof performance of the film was merely mentioned. Therefore, it is necessary to develop a strategy that can not only reduce the defects but also provide external hydrophobicity.

Multifunction molecular units with appropriate chain length are able to effectively passivate defects without hindering the

[a] Key Lab of Photovoltaic and Energy Conservation Materials, Institute of Solid State Physics, HFIPS, Chinese Academy of Sciences, Hefei 230031, China. E-mail: lhhu@rntek.cas.cn
[b] University of Science and Technology of China, No. 96 Jinzhai Road, Baohe District, Hefei, 230026, China
[c] National Center for Scientific Research "Demokritos", Institute of Nanoscience and Nanotechnology (INN), 153 10 Agia Paraskevi Attikis, Athens, Greece. E-mail: p.falaras@inn.demokritos.gr
[d] Greatcell Energy, 280 Byrnes Rd, Wagga Wagga, NSW, 2650, Australia

† Electronic supplementary information (ESI) available. See DOI: 10.1039/d1tc01720a

carrier injection from the perovskite material to the electron transport layer (ETL) or the hole transport layer (HTL). Based on this cogitation, the use of a multifunctional molecule to modify the interface defects and also offer a protective layer against humidity for the perovskite films is imperative. Chen *et al.* introduced multifunctional additive molecules containing long alkyl chains into perovskite precursor solution to both passivate the defects and block water penetration, thus improving the efficiency and stability of the PSCs simultaneously.[26] 1-Dodecanethiol (DDT) as a surface hydrophobic modifier with a long alkyl chain has been proved to be able to suppress defects by passivating perovskite. Uddin *et al.* carried out a series of surface ligand treatments for improving the optical properties of $CsPbBr_3$ nanocrystals (NCs). DDT produces NCs with the highest photoluminescence quantum yields (PLQY) and greatest long-term stability.[27] Park *et al.* passivated $CsPbBr_3$ quantum dots with DDT; the Br vacancies of PQDs were covered and the PLQY of DDT-PQDs improved from 76.1% to 99.8%.[28]

Herein, we employed the most known perovskite formulation, $(FAPbI_3)_{0.85}(MAPbBr_3)_{0.15}$, as the light absorption material. 1-Dodecanethiol (DDT) was used to passivate the surface and offer high hydrophobicity for perovskite films. It is found that the thiol group in DDT has a distinct ability to passivate the uncoordinated Pb^{2+} defects on perovskite surface *via* Lewis acid–base interactions. Furthermore, due to the existence of a long carbon chain, DDT improved the moisture stability of perovskite films simultaneously. Consequently, using this DDT passivation strategy, we achieved a high PCE exceeding 20% and a long-term stability of retaining 90% of initial PCE after 1000 hours aging in relative high humidity of $80 \pm 5\%$ without any encapsulation. This approach enlightens the efficacy of the application of multifunctional molecules in perovskite defect repair and advances research, with the aim to push forward practical applications in future.

Results and discussion

$(FAPbI_3)_{0.85}(MAPbBr_3)_{0.15}$ perovskite films were fabricated by the one-step anti-solvent assisted method which was previously reported in the literature.[29,30] As mentioned above, halide vacancies generated during PSC fabrication and subsequent operation can lead to the destruction of the PbX_6 octahedral arrangement or presence of uncoordinated Pb^{2+} sites.[10] To avoid these problems, an appropriate amount of DDT dissolved in the isopropyl alcohol (IPA) was introduced during post-treatment of the perovskite films through the dripping process before annealing. The film fabrication method is detailed in the Experimental section. DDT is an appropriate soft Lewis acid with a long alkyl chain of twelve carbon atoms and a terminal thiol group. Fig. 1 shows the schematic illustration of the detailed repair mechanism of DDT action on perovskite film. As reported in the previous literature,[28] the thiol group can fill the halide vacancies and bind with uncoordinated Pb^{2+}. The dodecyl long chain molecules with excellent hydrophobicity act like a "raincoat" draped on the surface of the perovskite film to prevent the destruction of the perovskite structure by water molecules, and thereby further improving structural stability.

X-Ray diffraction (XRD) measurements (Fig. 2a) were carried out to reveal crystallinity and phase transition of the perovskite absorber. DDT-*x* denote the different amounts of DDT dissolved in 1 ml IPA. Two dominant diffraction peaks located at 14.1° and 28.4° can be assigned to the (110) and (202) crystallographic phases of 3D perovskite, respectively.[31] As for the films with DDT post-treatment, there were no additional new peaks, which indicated that DDT passivation did not initiate phase transition or introduce the impurity phase to distort the crystal structure of perovskite. Notably, the peak intensity at 12.7° and 11.3° arising from PbI_2 and δ-phase perovskite was reduced in the film passivated using DDT at all concentrations, demonstrating that DDT passivation alleviated the formation of the non-perovskite phase and ameliorated crystallinity.[17,18,24] In this way, high-quality perovskite films were obtained. Preliminary experiments have shown that the concentration of DDT affects the whole performance of the device. Solutions with different concentrations of DDT in IPA were applied upon the surface of the perovskite films. The corresponding *J–V*

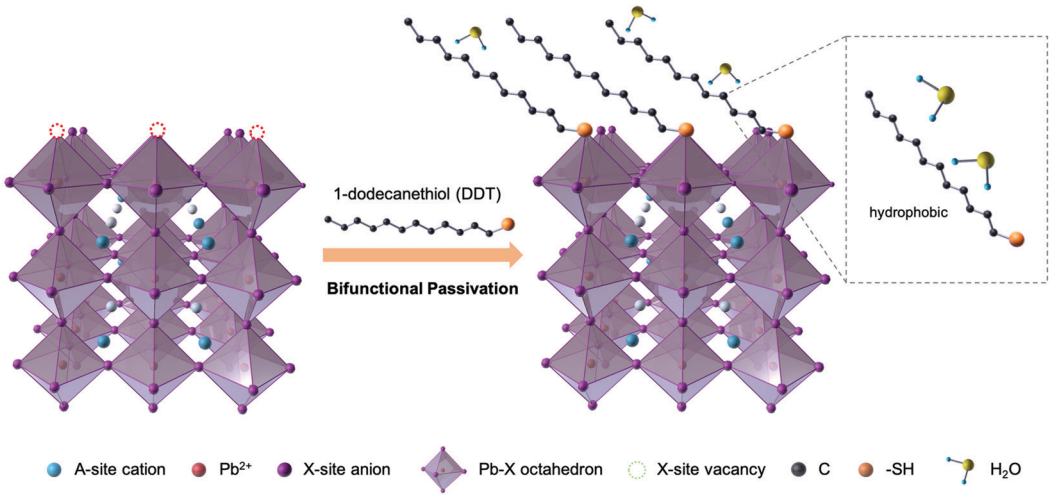

Fig. 1 Schematic representation of the DDT repair defects and humidity protection mechanism.

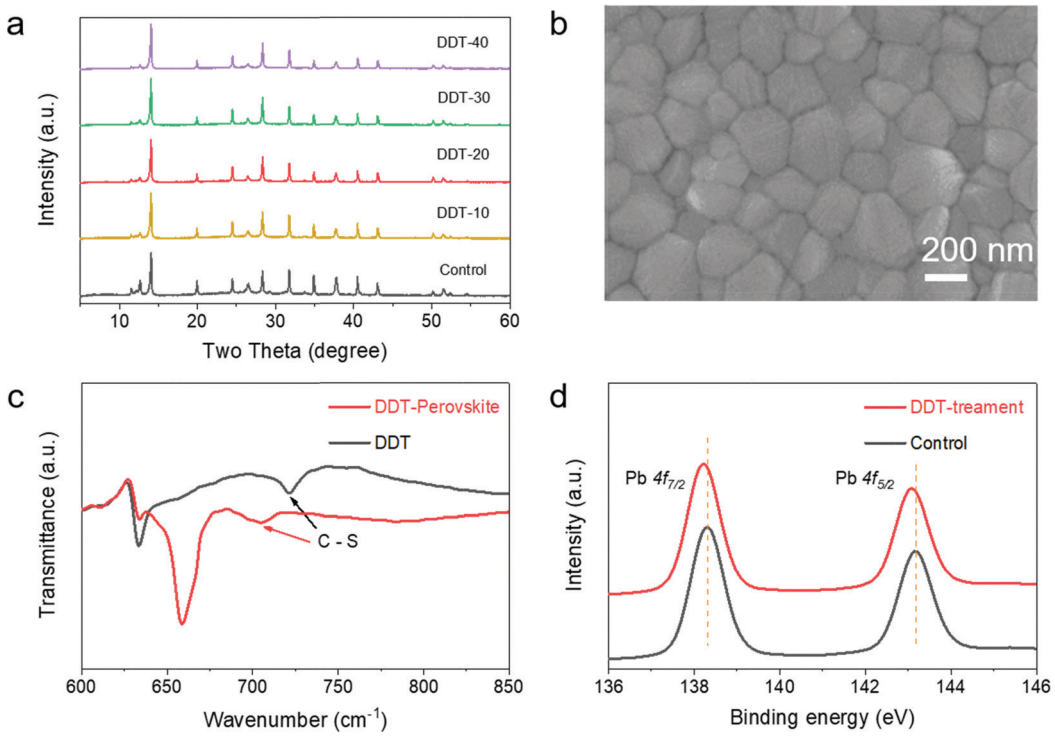

Fig. 2 (a) XRD patterns of control and DDT-*x* films (*x* = 10, 20, 30, 40). (b) SEM image of DDT-treated perovskite film. (c) Normalized Fourier transform infrared (FTIR) spectra of pure DDT and DDT–perovskite mixture solution. (d) X-Ray photoelectron spectroscopy (XPS) of the Pb 4f peak derived from the control and DDT-treated perovskite films.

curves are shown in Fig. S1 (in the ESI†) and the related parameters of the devices are listed in the image. It can be observed that the trend for PCE shows heads in different directions before and after DDT-20. Initially, the PCE increases with increase in DDT concentration, and this can be attributed to the progressive passivation of Pb^{2+} defects which reaches saturation at DDT-20. At concentrations greater than DDT-20, the high content of the long dodecyl alkyl chain will unavoidably affect the transport of the photogenerated carriers and this results in the observed decrease in the PCE. SEM images did not show any obvious difference in perovskite surface morphologies after DDT-treatment (Fig. 2b and Fig. S2, ESI†). DDT-treatment had a little effect on the morphology of the film. When an appropriate amount of DDT is used for passivation, the irregular small grains on the perovskite surface tend to disappear. In order to explore the effect of DDT-treatment, FTIR characterization was carried out. Fig. 2c exhibits the FTIR spectra of pure DDT and the interaction between DDT and perovskite. The C–S vibration peaks observed in the FTIR spectra red-shifted from 721 cm^{-1} to 706 cm^{-1} with the formation of DDT–perovskite complex, which confirmed the existence of Lewis acid–base interactions between thiol from DDT and PbI_2.[32] To further explore the mechanism of DDT passivation on the perovskite, XPS measurement were conducted. There was almost no S signal in the control film, and a weak S 2p peak appeared at 163.7 eV in the film after DDT treatment, which is an evidence of the existence of DDT on the modified surface (Fig. S3, ESI†). In the control perovskite film, the Pb 4f peaks were located at 138.3 eV (Pb $4f_{7/2}$) and 143.2 eV (Pb $4f_{5/2}$). In DDT-treated perovskite film, the Pb 4f peaks shifted to 138.2 eV and 143.0 eV. The spin–orbit splitting between the Pb $4f_{7/2}$ and Pb $4f_{5/2}$ levels in all cases remains at *ca.* 4.8 eV, which is in accordance with the literature values, suggesting that the Pb in the films acts as the oxidation state of Pb^{2+}.[33] Since XPS is mainly able to detect the surface species, we propose that the shift of the Pb 4f orbital is caused by the DDT surface treatment. Owing to the electron donating properties of Lewis base, the Pb^{2+} peaks shifted to a lower binding energy, indicating that the uncoordinated Pb^{2+} in the perovskite film interacts with the SH ligand.[10,32]

It was well demonstrated that defect concentration is related with carrier recombination inseparably in perovskite films, which seriously affects the extraction and transport of charge carriers. To investigate the effect of DDT on charge carrier dynamics, ultraviolet-visible (UV-vis) absorption spectra, steady-state photoluminescence (PL) and time-resolved photoluminescence (TRPL) measurements were conducted. Fig. 3a displays the UV-vis spectra and PL spectra of pristine and DDT-treated films deposited on FTO glass. We can observe that the absorption edges of the perovskite films with and without treatment of DDT are located at ~786 and ~780 nm, respectively, which correspond to the red-shift in the PL spectra. Depending on the experimental conditions and molecular nature, the addition of surface modifiers might cause the blue shift of PL, or bring the red shift or even have no effect on the PL peak position. As discussed by Park *et al.*,[28] $CsPbBr_3$ treated

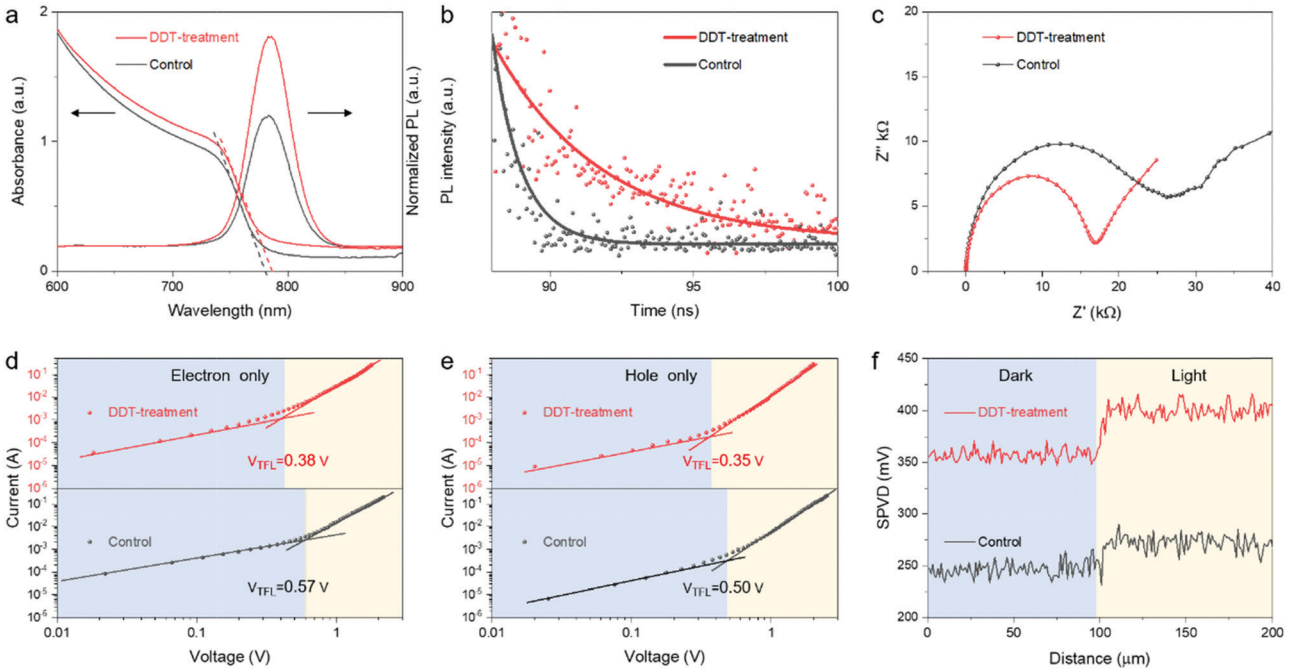

Fig. 3 (a) UV-vis spectra (left), PL spectra (right) and (b) normalized time-resolved photoluminescence of control and DDT-treated perovskite films. (c) Nyquist plots of the control and modified devices at $V = -0.8$ V in the dark. The space charge limited current *versus* voltage of (d) electron-only devices and (e) hole-only devices for the control and after DDT-treatment. (f) Surface photovoltage of the control and DDT-treated perovskite films under dark and light illumination.

with 1-dodecanethiol also had a PL red-shift, which was attributed to the quantum confinement effects following the SH ligand passivation process. In addition, a red-shift of the PL was also observed following the hexylammonium iodide post deposition treatment on top of already crystalized $Cs_{0.2}FA_{0.8}Pb(I_{0.8}Br_{0.2})_3$ 3D perovskite.[34] To explain this effect, the authors made the assumption of halide exchange at the perovskite interface during a liquid–solid reaction and/or the annealing stage. The PL intensity of perovskite film was enhanced after DDT-treatment under a 470 nm excitation light. It is expected that only the perovskite surface (<100 nm) will be excited because of its strong absorption coefficient at short wavelength range.[35] Therefore, trap-state density on the perovskite surface was significantly reduced, in agreement with the observation of a stronger PL intensity peak. Generally, the defect states in perovskite films serve as non-radiative recombination centers which ultimately reduce the device performance. The mitigation of surface defects prolongs the PL lifetime of perovskite films. Correspondingly, the carrier lifetime values of the pristine and modified films were calculated by fitting the time-resolved photoluminescence (TRPL) spectra (Fig. 3b) with a single exponential decay function:[36]

$$y = A_1 \times \exp(-x/\tau_1) + y_0$$

where A_1 is the time-independent coefficient of amplitude fraction and τ_1 is the carrier lifetime. According to the results, the carrier lifetime of the modified perovskite films increased from 1.18 ns to 3.75 ns. The increased carrier lifetime arose from DDT amelioration of non-radiative recombination which is due to the repair of various defects in the perovskite films.[24] Electrochemical impedance spectroscopy (EIS) measurement was conducted to investigate the transport and recombination resistance in PSCs. The Nyquist plots (Fig. 3c) of control and DDT-treated devices were collected at a frequency range of 1 Hz–100 kHz and excitation voltage at −0.8 V in the dark. Both curves consist of a semicircle in the high frequency region and a steep straight line in the low frequency region. The diameter of the semicircle in the high frequency region represents the charge transfer resistance (R_{ct}).[18] By comparing the Nyquist curves, it can be observed that the R_{ct} of modified PSC is much smaller than that of the control device, which was because the charge transfer in the perovskite films was ameliorated due to DDT modification.

The space charge limited current (SCLC) technique was employed to explore the electron trap density of pristine and DDT-treated perovskite films. Fig. 3d and e illustrate the dark current–voltage characteristics of electron-only devices (FTO/c-TiO_2/mp-TiO_2/perovskite/PCBM/Au) and hole-only devices (FTO glass/PEOOT:PSS/perovskite/PCBM/Spiro-OMeTAD/Au) with and without DDT treatment. The limit voltage (V_{TFL}) is correlated with defect trap density (N_{trap}) through the following equation:[20,37]

$$N_{trap} = (2\varepsilon\varepsilon_0 V_{TFL})/(eL^2)$$

where ε_0 is the vacuum permittivity, ε is the relative dielectric constant, e is the elemental charge, and L is the thickness of the perovskite film, calculated to be *ca.* 550 nm from the cross-SEM section images of the PSC device (Fig. S4, ESI†). V_{TFL} is the

onset voltage of the trap filled limit region. The V_{TFL} values were calculated to be 0.57 V and 0.38 V for the control and DDT treated devices by fitting the dark J–V curves, respectively. The trap density of the corresponding electron-only device is reduced from 6.94×10^{15} cm^{-3} to 4.62×10^{15} cm^{-3} after DDT passivation. The V_{TFL} and N_{trap} of hole-only devices with DDT treatment were 0.35 V and 4.25×10^{15} cm^{-3} which was lower than 0.50 V and 6.08×10^{15} cm^{-3} of the control device, indicating that the hole transport hindrance of the modified device was reduced. The reduced defect density could be attributed to the defect-passivation of perovskite films by DDT treatment and was consistent with the PL and TRPL results.[18,21] Kelvin probe force microscopy (KPFM) was used to detect the surface potential distribution of the perovskite films. The mean contact-potential-difference (V_{CPD}) is defined as: $V_{CPD} = (\Phi_{tip} - \Phi_{sample})/-e$, where Φ_{tip} and Φ_{sample} are the work functions of the AFM tip and measured sample, and e is the elementary charge.[38] Since Φ_{tip} and e were constant, the change of V_{CPD} reflects the change in the work function of the sample surface. The surface photovoltage (SPV) is the difference of surface potential under dark and illumination:[39] $SPV = V_{(CPD)light} - V_{(CPD)dark}$. SPV is generated by the transfer and separation process of charge carriers, leading to the redistribution of charges and accumulation of surface dipole in the space charge region.[40] Therefore, SPV is related to the charge carriers' transport and its magnitude represents the density of surface trap states. In Fig. 3f, the SPV of control device and DDT-treated device were 27.1 mV and 44.8 mV. A larger SPV

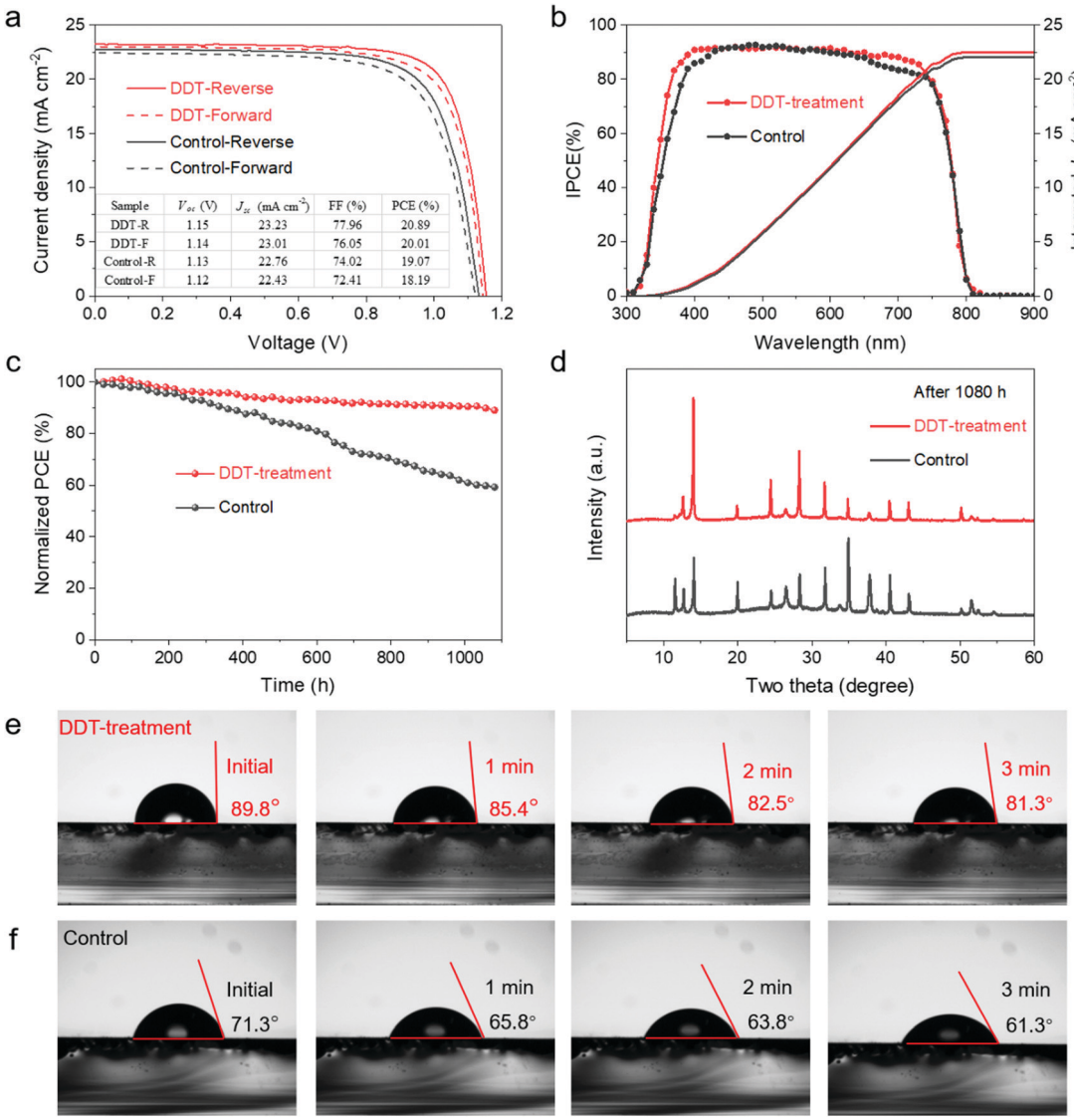

Fig. 4 (a) J–V curves of the control and modified PSCs under reverse and forward scan directions. (b) IPCE spectra and the integrated J_{sc} of the control and modified PSCs. (c) The humidity stability results of PSCs based on control and DDT-treated devices after 1000 hours under relative humidity conditions of 80 ± 5% without encapsulation at room temperature (in dark). (d) XRD patterns of the control and modified perovskite films after aging under 80 ± 5% RH for 1000 hours. The water contact angle of (e) DDT-treated and (f) control perovskite films with different exposure time periods.

value indicates that more charge could be transferred from inside of the film to the surface and could be extracted and collected at the electrodes.

To confirm the effectiveness of DDT on the photovoltaic performance, PSCs with a multilayered structure of FTO/c-TiO_2/m-TiO_2/perovskite/DDT/Spiro-OMeTAD/Au were fabricated, and the corresponding cell architecture is shown in Fig. S5 (ESI†). The photovoltaic performance of the control and modified PSCs was measured under a standard AM 1.5 simulated solar light illumination with an active area of 0.09 cm^{-2}. Fig. 4a illustrates the corresponding current–voltage (J–V) curves. The photovoltaic parameters of the corresponding control and DDT-treated devices are listed in the figure inset. The modified device exhibits a V_{oc} of 1.15 V, a J_{sc} of 23.23 mA cm^{-2} and a fill factor (FF) of 77.96%, yielding a high PCE of 20.89%. Referring to the control device, the PCE is 19.07% with a V_{oc} of 1.13 V, a J_{sc} of 22.76 mA cm^{-2} and an FF of 74.02%. Moreover, the I–V hysteresis factor (HF) which is defined as:[41]

$$HF = (PCE_{reverse} - PCE_{forward})/PCE_{reverse}$$

was also calculated. The modified cells have a HF of 4.21%, which is slightly better than that of the control cells (4.61%). The significant improvement of the DDT device performance about 10% higher than that of the control PSC is due to the trap-state passivation effect and carrier extraction enhancement. The corresponding incident photon-to-current conversion efficiency (IPCE) spectra were registered to evaluate the photon energy response of the devices. As shown in Fig. 4b, the modified PSCs display higher response than the control device within the wavelength ranging from 350 to 780 nm. The integrated J_{sc} values of control and modified devices are calculated to be 22.06 and 22.54 mA cm^{-2}, respectively, which are in good agreement with the J_{sc} values obtained from the J–V curves. The uniformity and reproducibility of the control and DDT-treated PSCs were further analyzed by a series of produced devices involving 20 individual devices. As shown in Fig. S6 (ESI†), the average PCE of DDT-treated devices has increased from 18.48% to 20.15% due to the corresponding increase in V_{oc},J_{sc} and FF; importantly, all the parameters showed a narrow distribution. These results proved that the device performance can be improved with high reproducibility by DDT passivation of the perovskite absorber.

For practical applications, environmental stability, especially humidity stability, is a critical indicator to evaluate the performance of PSCs. Although the cells based on mixed FA–MA perovskite possess excellent PCE, humidity induced phase transition from α-phase to δ-phase further degrade to PbI_2 and made devices unstable.[42] In the process of DDT repaired defects, dodecyl was like a ''raincoat'' draped on the surface of perovskite. Due to the excellent hydrophobicity of the dodecyl alkyl chain, the perovskite would suffer less moisture invasion. Thus, the devices treated with DDT were expected to have good humidity stability. In order to evaluate humidity stability improvement of the DDT-treated perovskites, the control and DDT-treated devices without any encapsulation were exposed to relative humidity of 80 ± 5% at room temperature under dark conditions. As shown in Fig. 4c, the control device showed a faster PCE decay rate than the DDT-treated device from the outset of testing, and finally lost about 40% of the initial efficiency after the 1000 h humidity aging process. The XRD patterns (Fig. 4d) of the corresponding control film obtained following humidity aging suggest that the perovskite α-phase was gradually transformed to the δ-phase perovskite accompanied by the increase in the formation of the degradation product PbI_2. On the contrary, the XRD pattern of the DDT-treated film in the humidity aging test showed less phase transition and less PbI_2 generation after 1000 h aging, indicating that DDT treatment significantly enhanced humidity resistance. As a result, DDT-treated devices maintained more than 90% initial efficiency after humidity aging for 1000 hours. To further investigate the hydrophobicity of the passivated devices, water contact angle measurement tests were conducted. Fig. 4e and f illustrate the evolution of water contact angle with respect to time. At the beginning, the modified films are more hydrophobic, presenting a large water contact angle of 89.8°, while the corresponding value for the control film was only 71.3°. The hydrophobicity of the films did not significantly vary with increase in time: the film treated with DDT could retain 81.3° after 3 min, while the angle of the pristine film decreased from 71.3° to 61.3° already. This phenomenon proved that DDT treatment will bring excellent humidity protection performance to the perovskite film. Compared with that of the control film, the improved hydrophobicity of the DDT-treated films was attributed to the presence of water repelling long dodecyl chains. These results are consistent with the humidity stability of the corresponding devices.

Conclusion

In summary, we employed 1-dodecanethiol (DDT) as a dual-functional modifier to enhance the performance and stability of PSCs. One clear effect of functionalizing the perovskite with DDT is the repair of halide vacancies and the corresponding uncoordinated Pb^{2+} defects, yielding better carrier transport and extraction. Another effect is the protection of the perovskite from the damage caused by water molecules. As a result, control devices afforded a PCE of 19.07% and 40% initial performance loss after 1000 h aging at a relative humidity of 80 ± 5%. DDT-treated devices delivered a remarkable PCE of 20.89% and maintained over 90% of their initial performance under the same aging conditions. These results demonstrate that the multifunctional molecular modifier DDT can be used to repair defects in PSCs and provide a unique and synergistic performance enhancing humidity stability.

Conflicts of interest

There are no conflicts of interest to declare.

Acknowledgements

This work was supported by the National Key R&D Program of China (2017YFE0133800), the National Natural Science Foundation of China (51961165106), Anhui Provincial Natural Science Foundation (1908085QB52), and European Union's HORIZON 2020 Marie Curie Innovative Training Network 764787 MAESTRO project.

References

1 X. Xu, Y. Sun, D. He, Z. Liang, G. Liu, S. Xu, Z. Li, L. Zhu and X. Pan, *J. Mater. Chem. C*, 2021, **9**, 208–213.
2 S. Yuan, Y. Cai, S. Yang, H. Zhao, F. Qian, Y. Han, J. Sun, Z. Liu and S. (Frank) Liu, *Sol. RRL*, 2019, **3**, 1900220.
3 L. Fu, H. Li, L. Wang, R. Yin, B. Li and L. Yin, *Energy Environ. Sci.*, 2020, **13**, 4017–4056.
4 J. J. Yoo, G. Seo, M. R. Chua, T. G. Park, Y. Lu, F. Rotermund, Y. Kim, C. S. Moon, N. J. Jeon, J. Correa-Baena, V. Bulović, S. S. Shin, M. G. Bawendi1 and J. Seo, *Nature*, 2021, **590**, 587–593.
5 B. Chaudhary, T. M. Koh, B. Febriansyah, A. Bruno, N. Mathews, S. G. Mhaisalkar and C. Soci, *Sci. Rep.*, 2020, **10**, 429.
6 J. Hu, C. Wang, S. Qiu, Y. Zhao, E. Gu, L. Zeng, Y. Yang, C. Li, X. Liu, K. Forberich, C. J. Brabec, M. K. Nazeeruddin, Y. Mai and F. Guo, *Adv. Energy Mater.*, 2020, 2000173.
7 T. M. Koh, V. Shanmugam, X. Guo, S. S. Lim, O. Filonik, E. M. Herzig, P. Müller-Buschbaum, V. Swamy, S. T. Chien, S. G. Mhaisalkar and N. Mathews, *J. Mater. Chem. A*, 2018, **6**, 2122–2128.
8 M. I. Saidaminov, J. Kim, A. Jain, R. Quintero-Bermudez, H. Tan, G. Long, F. Tan, A. Johnston, Y. Zhao, O. Voznyy and E. H. Sargent, *Nat. Energy*, 2018, **3**, 648–654.
9 W. Zhao, J. Shi, C. Tian, J. Wu, H. Li, Y. Li, B. Yu, Y. Luo, H. Wu, Z. Xie, C. Wang, D. Duan, D. Li and Q. Meng, *ACS Appl. Mater. Interfaces*, 2021, **13**, 9771–9780.
10 Z. Wu, M. Jiang, Z. Liu, A. Jamshaid, L. K. Ono and Y. Qi, *Adv. Energy Mater.*, 2020, **10**, 1903696.
11 K. Zhang, Z. Wang, G. Wang, J. Wang, Y. Li, W. Qian, S. Zheng, S. Xiao and S. Yang, *Nat. Commun.*, 2020, **11**, 1006.
12 R. Long, J. Liu and O. V. Prezhdo, *J. Am. Chem. Soc.*, 2016, **138**, 3884–3890.
13 S. Ye, H. Rao, Z. Zhao, L. Zhang, H. Bao, W. Sun, Y. Li, F. Gu, J. Wang, Z. Liu, Z. Bian and C. Huang, *J. Am. Chem. Soc.*, 2017, **139**, 7504–7512.
14 L. Ruan, W. Shen, A. Wang, Q. Zhou, H. Zhang and Z. Deng, *Nanoscale*, 2017, **9**, 7252–7259.
15 M. Vasilopoulou, A. Fakharuddin, A. G. Coutsolelos, P. Falaras, P. Argitis, A. R. M. Yusoff and M. K. Nazeeruddin, *Chem. Soc. Rev.*, 2020, **49**, 4496–4526.
16 N. Balis, A. H. Zaky, D. Perganti, A. Kaltzoglou, L. Sygellou, F. Katsaros, T. Stergiopoulos, A. G. Kontos and P. Falaras, *ACS Appl. Energy Mater.*, 2018, **1**, 6161–6171.
17 A. A. Zaky, N. Balis, K. Gkini, C. Athanasekou, A. Kaltzoglou, T. Stergiopoulos and P. Falaras, *ChemistrySelect*, 2020, **5**, 4454–4462.
18 M. Elsenety, A. Stergiou, L. Sygellou, N. Tagmatarchis, N. Balis and P. Falaras, *Nanoscale*, 2020, **12**, 15137–15149.
19 K. Gkini, N. Balis, M. Papadakis, A. Verykios, M. Scoulicidou, C. Drivas, S. Kennou, M. Golomb, A. Walsh, A. G. Coutsolelos, M. Vasilopoulou and P. Falaras, *ACS Appl. Energy Mater.*, 2020, **3**, 7353–7363.
20 N. Balis, A. A. Zaky, C. Athanasekou, A. M. T. Silva, E. Sakellis, M. Vasilopoulou, T. Stergiopoulos, A. G. Kontos and P. Falaras, *J. Photochem. Photobiol., A*, 2020, **386**, 112141.
21 A. A. Zaky, E. Christopoulos, K. Gkini, M. K. Arfanis, L. Sygellou, A. Kaltzoglou, A. Stergiou, N. Tagmatarchis, N. Balis and P. Falaras, *Appl. Catal., B*, 2021, **284**, 119714.
22 H. Zheng, G. Liu, L. Zhu, J. Ye, X. Zhang, A. Alsaedi, T. Hayat, X. Pan and S. Dai, *ACS Appl. Mater. Interfaces*, 2017, **9**, 41006–41013.
23 H. Zheng, G. Liu, X. Chen, B. Zhang, A. Alsaedi, T. Hayat, X. Pan and S. Dai, *J. Mater. Chem. A*, 2018, **6**, 20233–20241.
24 M. M. Elsenety, M. Antoniadou, N. Balis, A. Kaltzoglou, L. Sygellou, A. Stergiou, N. Tagmatarchis and P. Falaras, *ACS Appl. Energy Mater.*, 2020, **3**(3), 2465–2477.
25 M. Dehghanipour, A. Behjat and H. A. Bioki, *J. Mater. Chem. C*, 2021, **9**, 957–966.
26 L. Zhu, X. Zhang, M. Li, X. Shang, K. Lei, B. Zhang, C. Cong, S. Zheng, H. Song and J. Chen, *Adv. Energy Mater.*, 2021, **11**, 2100529.
27 M. A. Uddin, J. K. Mobley, A. A. Masud, T. Liu, R. L. Calabro, D.-Y. Kim, C. I. Richards and K. R. Graham, *J. Phys. Chem. C*, 2019, **123**, 18103–18112.
28 S. Park, H. Cho, W. Choi, H. Zou and D. Y. Jeon, *Nanoscale Adv.*, 2019, **1**, 2828–2834.
29 H. Xu, Y. Sun, H. Zheng, G. Liu, X. Xu, S. Xu, L. Zhang, X. Chen and X. Pan, *J. Mater. Chem. C*, 2019, **7**, 15276–15284.
30 M. Konstantakou, D. Perganti, P. Falaras and T. Stergiopoulos, *Crystals*, 2017, **7**(10), 291.
31 M. Hu, L. Zhang, S. She, J. Wu, X. Zhou, X. Li, D. Wang, J. Miao, G. Mi, H. Chen, Y. Tian, B. Xu and C. Cheng, *Sol. RRL*, 2019, 1900331.
32 D. Bi, X. Li, J. V. Milić, D. J. Kubicki, N. Pellet, J. Luo, T. LaGrange, P. Mettraux, L. Emsley, S. M. Zakeeruddin and M. Grätzel, *Nat. Commun.*, 2018, **9**, 4482.
33 R. Lindblad, D. Bi, B-w. Park, J. Oscarson, M. Gorgoi, H. Siegbahn, M. Odelius, E. M. J. Johansson and H. Rensmo, *J. Phys. Chem. Lett.*, 2014, **5**, 648–653.
34 S. Rahmany and L. Etgar, *Mater. Adv.*, 2021, **2**, 2617–2625.
35 Q. Jiang, Y. Zhao, X. Zhang, X. Yang, Y. Chen, Z. Chu, Q. Ye, X. Li, Z. Yin and J. You, *Nat. Photonics*, 2019, **13**, 460–466.
36 G. Xing, N. Mathews, S. Sun, S. S. Lim, Y. M. Lam, M. Grätzel, S. Mhaisalkar and T. C. Sum, *Science*, 2013, **342**, 344.

37 J. Chen, S. Kim, X. Ren, H. S. Jung and N. Park, *J. Mater. Chem. A*, 2019, **7**, 4977–4987.
38 Y. Rosenwaks and R. Shikler, *Phys. Rev. B: Condens. Matter Mater. Phys.*, 2004, **70**, 085320.
39 H. Yi, L. Duan, F. Haque, J. Bing, J. Zheng, Y. Yang, A. C. Mo, Y. Zhang, C. Xu, G. Conibeer and A. Uddin, *J. Power Sources*, 2020, **466**, 228320.
40 Y. Almadori, D. Moerman, J. L. Martinez, P. Leclère and B. Grévin, *Beilstein J. Nanotechnol.*, 2018, **9**, 1695–1704.
41 M. M. Elsenety, M. Antoniadou, N. Balis, A. Kaltzoglou, L. Sygellou, A. Stergiou, N. Tagmatarchis and P. Falaras, *ACS Appl. Energy Mater.*, 2020, **3**, 2465–2477.
42 G. Liu, H. Zheng, X. Xu, S. Xu, X. Zhang, X. Pan and S. Dai, *Adv. Funct. Mater.*, 2019, 1807565.